Received: 26 November 2019 | Revised: 30 September 2020 | Accepted: 6 October 2020 | Published on: 21 October 2020

DOI: 10.1002/joc.6874

RESEARCH ARTICLE

International Journal of Climatology RMetS

A new approach to classification of 40 years of Antarctic sea ice concentration data

Paul Wachter[1] | **Fabian Reiser**[2] | **Peter Friedl**[3] | **Jucundus Jacobeit**[4]

[1]German Aerospace Center (DLR), German Remote Sensing Data Center (DFD), Wessling, Germany

[2]Department of Environmental Meteorology, University of Trier, Trier, Germany

[3]Institute of Geography, Friedrich-Alexander-University Erlangen-Nuremberg, Erlangen, Germany

[4]Institute of Geography, Augsburg University, Augsburg, Germany

Correspondence
Paul Wachter, German Aerospace Center (DLR), German Remote Sensing Data Center (DFD), D-82234 Wessling, Germany.
Email: paul.wachter@dlr.de

Funding information
DLR Management Board: Young Investigator Group Leader Program. F.R. was funded by the Deutsche Forschungsgemeinschaft, Grant/Award Number: WI 3314/3 and HE 2740/22

Abstract

In this paper, we present a characterization of Antarctic sea ice based on the classification of annual sea ice concentration (SIC) data from 1979 to 2018. A clustering algorithm was applied to provide a climatological description of significant annual cycles of SIC and their spatial distribution around the Southern Ocean. Based on these classification results, we investigate the variability of SIC cycles on decadal and inter-annual time scales. First, we discuss significant spatial shifts of SIC cycles during 1979–1998 and 1999–2018. In the Weddell Sea and in large parts of the Ross Sea, we observed higher SIC during the summer season, and an extension of sea ice cover in winter compared to the long-term average. Second, we introduce the Climatological Sea Ice Anomaly Index (CSIAI), which is an annual measure for year-round sea ice anomalies of the Southern Ocean and its regional sub-sectors. By relating selected years of significant sea ice conditions (1981, 2007 and 2014) with atmospheric influences, we demonstrate that the CSIAI is very useful for assessing inter-annular Antarctic SIC variability. Positive and negative sea ice anomalies can be qualitatively explained by atmospheric circulation anomalies in the years 1981 and 2007. However, in 2014, the year with the largest observed sea ice extent in our time series, we found that this positive sea ice anomaly was surprisingly not associated with a stationary and inter-seasonally persistent pattern of circulation anomaly. This suggests that sub-seasonal to seasonal circulation anomalies and ocean-related processes favoured the formation of the sea ice maximum in 2014. With this study we provide additional information on the long-term annual SIC variability around Antarctica. Furthermore, our classification approach and its results have potential for application in the evaluation of sea ice model results.

KEYWORDS

passive microwave data, sea ice climatology, sea ice trends, sea ice variability

1 | INTRODUCTION

Sea ice plays an important role in the global climate system because it acts as an insulator and prevents the ocean from losing heat and moisture, particularly during winter, to the atmosphere (Maykut, 1982). The high albedo of sea ice, in contrast to the low albedo of open water, reflects up to 90% of incoming shortwave radiation, thereby preventing its absorption at the surface (King and Turner, 1997). Both the melting and the formation of sea ice interact with ocean circulation, for example, by increasing the salt concentration due to the release of brine during the formation of ice, which contributes to the formation of dense water and consequently to deep-ocean bottom water circulation (Smith *et al*., 1990; Gordon *et al*., 2007). Furthermore, sea ice is also a habitat for mammals and sea birds, and it in turn affects the oceanic biological productivity due to its high spatial and temporal variability (e.g., Eicken, 1992 and references therein).

Sea ice covers large areas of the Southern Ocean and shows high seasonal variability (Zwally *et al*., 2002). The sea ice extent (SIE) varies between 2.07×10^6 km^2 in late summer (March 1, 2017, Turner *et al*., 2017) and 20.14×10^6 km^2 in late winter (September 20, 2014, Turner *et al*., 2015). From a long-term perspective, the sea ice concentration (SIC) in the Ross Sea, the Weddell Sea, and most parts of the East Antarctic sector increased significantly during the period 1979–2013 (Turner *et al*., 2015; Hobbs *et al*., 2016). However, not all regions show a positive trend in SIC. In particular, the Amundsen and Bellingshausen Seas are dominated by a decrease in SIC, which is significant in autumn and summer. A recent study by Parkinson (2019) confirmed the general trend characteristics of Antarctic sea ice but draws further attention on a precipitous negative SIE in the years since 2014. In this study, she concluded that the trend in SIE from 1979 to 2018 was only 50% of the trend for the period from 1979 to 2014. According to Meehl *et al*. (2019), these negative SIE anomalies in recent years have been caused by upwelling of warm subsurface waters. The negative SIE in the Weddell Sea since 2016 has been described by Turner *et al*. (2020), who relate the recent sea ice anomaly with strong westerly winds and the reappearance of the Maud Rise Polynya.

In addition to trend analyses of the long-term development of SIE, other studies have focused on changes in the length of the sea ice season (Stammerjohn *et al*., 2008). Simpkins *et al*. (2013) demonstrated that the Amundsen and Bellingshausen Seas were particularly affected by a decline in the duration of sea ice seasons from 1979 to 2012. This negative trend is caused by a later advance and an earlier retreat of sea ice. In the Weddell and Ross Sea sectors, however, a positive trend towards longer sea ice seasons has been observed (Simpkins *et al*., 2013).

Much attention was given to the influence of atmospheric variables on spatial and temporal variability of Antarctic sea ice. Holland and Kwok (2012) showed that in large areas of the Southern Ocean, sea ice drift is correlated with the speed and direction of surface wind patterns. Comiso *et al*. (2017) showed that negative near-surface temperature trends are associated with positive trends in sea ice cover. The intensities and spatial variations of these near-surface parameters are driven by large-scale atmospheric circulation. Variability in the Southern Hemisphere atmospheric circulation can be described by the Southern Annular Mode (SAM) Index or by the El Niño Southern Oscillation (ENSO) Index. Stammerjohn *et al*. (2008) showed that La Niña Events during positive SAM periods led to an earlier retreat and later advance of sea ice at the western Antarctic Peninsula and the Bellingshausen Sea. Simmonds and Jacka (1995) identified a time-shifted positive correlation between the Southern Oscillation and Southern Hemispheric SIE. Other atmospheric circulation patterns, including the quasi-stationary Amundsen Sea Low (Turner *et al*., 2017), the zonal wave three (Schlosser *et al*., 2018) and the semiannual oscillation (van den Broeke, 2000), also influence the distribution of Antarctic sea ice.

Recent developments in Antarctic SIE, especially the extreme negative sea ice anomaly in 2016/2017, have attracted attention. In Turner *et al*. (2017), a historically low pressure in the Amundsen Sea was identified as the reason for an enhanced sea ice retreat in the Amundsen, Bellingshausen, and Weddell Seas in this season. They concluded that the anomalously strong springtime SIE retreat was caused by intense planetary wave (PW) activity associated with a strong poleward heat flux. Schlosser *et al*. (2018) discussed the important role of strong positive zonal wave three activity and negative SAM for the 2016/2017 sea ice anomaly. However, Schlosser *et al*. (2018) and Stuecker *et al*. (2017) also concluded that preconditioning processes in the Atmosphere—Sea Ice—Ocean system, for example, the strong 2015/2016 El Niño event, might have affected this distinctive Antarctic sea ice anomaly.

As suggested by different studies, additional processes need to be included to fully explain the temporal and spatial variance in Antarctic SIE. In Turner *et al*. (2009) and Sigmond and Fyfe (2014), emphasis was placed on ozone depletion in the Southern Hemisphere (SH) and possible interactions with SIE. Turner *et al*. (2009) showed that ozone depletion caused a deepening of the Amundsen low, which resulted in increased SIE in the Ross Sea.

Most of the studies mentioned above used SIC and SIE derived from satellite passive microwave data for long-term trend analysis of Antarctic sea ice or to investigate individual, seasonal sea ice anomaly events. To our knowledge, up to now there are no studies that address significant spatio-temporal characteristics of annual SIC over the entire Southern Ocean from a climatological perspective. In this study, we employed a novel classification-based approach applied on passive microwave SIC data to investigate annual cycles of SIC (hereafter "sea ice classes") in the Southern Ocean (Section 2). With this classification, we aim at identifying significant sea ice classes that are representative for the entire annual sea ice cycle of the Southern Ocean over the past four decades. This climatological approach provides a comprehensive description of the spatial distribution patterns of sea ice classes and serves as a reference for additional investigations of temporal variability and spatial trends of the identified sea ice classes (Section 3). Since the sea ice classes identified in this study represent significant annual SIC cycles, changes in spatial distribution patterns are clear indications of climatically relevant trends in Antarctic sea ice. Our classification-based consideration of entire annual cycles reduces the influence of short-term SIC fluctuations and focuses on climatologically relevant annual anomalies and long-term trends. With our newly developed Climatological Sea Ice Anomaly Index (CSIAI), the inter-annual sea ice variability can be assessed and significant years of Antarctic sea ice anomalies are identified. Selected years of remarkable sea ice class anomalies—as indicated by the CSIAI—are presented and the possible influences of atmospheric circulation anomalies are discussed. These synoptic considerations demonstrate the sensitivity of our methodology to atmospherically induced sea ice anomalies. Section 4 concludes this study and discusses possible future applications of the proposed methodology and the derived results.

2 | DATA AND METHODS

2.1 | Sea ice data

We used data from January 1979 to December 2018 derived by the NASA Team (NT) sea ice algorithm (Version 1.1, Cavalieri *et al*., 1996), which provides daily, quality-controlled, SIC data since 1979 and is updated every year. Based on this data product, it is possible to analyse the full annual cycles of sea ice for the SH over the last four decades. The SIC is defined as the percentage of a pixel (nominal grid resolution of 25 km × 25 km) covered with sea ice. Figure 1 shows the data availability of the NT dataset, which consists of data acquired by three different passive microwave sensors during six successive satellite missions. The Scanning Multichannel Microwave Radiometer (SMMR) on board Nimbus-7 delivered the first data set on October 26, 1978. The subsequent Defence Meteorological Satellite Program (DMSP) satellite platforms (F8, F11, and F13) operated the Special Sensor Microwave Imager/Sounder (SSM/I). The latest instrument generation, the Special Sensor Microwave Imager/Sounder (SSMI/S), was operated on the DMSP-F17 platform.

During the first phase of the study period, the SIC data products for the Nimbus-7 acquisitions are available every second day. Since August 20, 1987, SIC data are

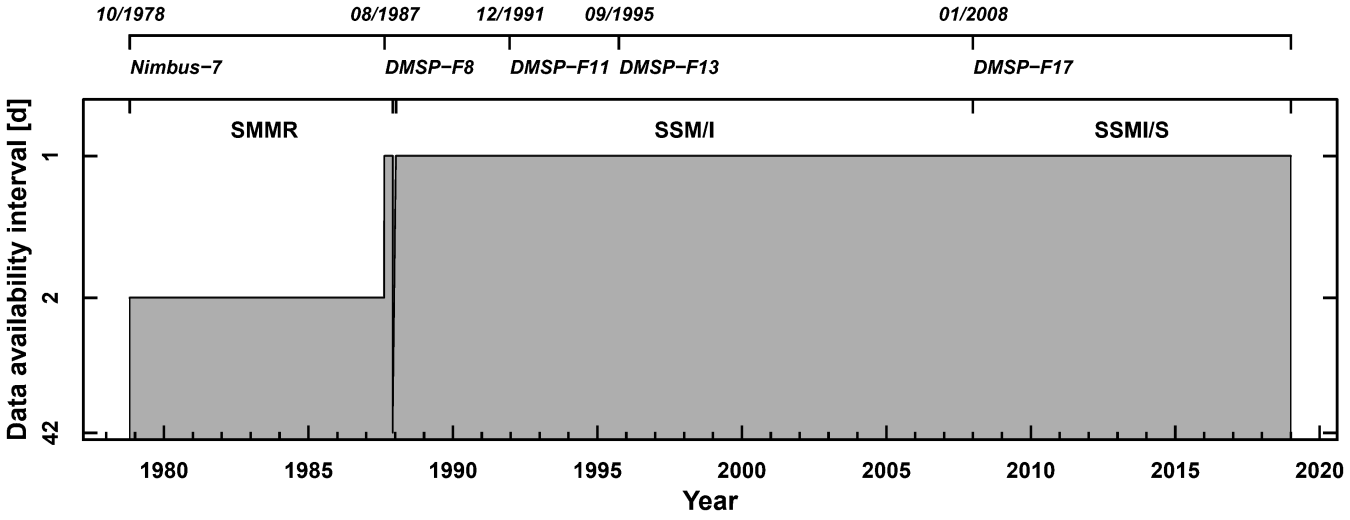

FIGURE 1 Timeline of passive microwave sensors operated on different satellite platforms since October 1978. The graphic shows the data availability interval of the NASA Team sea ice concentration data product (version 1.1) as it is provided by Cavalieri *et al*. (1996)

available on a daily basis. A single data gap of 41 missing days exists between December 3, 1987 and January 12, 1988. Due to the data availability interval of 2 days from October 1978 to August 1987 and the 41 days data gap in 1987–88 we interpolated the dataset to obtain an equidistant, daily data time series. Missing SIC data fields were filled by linear interpolation between the preceding and subsequent SIC data fields. The original data fields (316 columns and 332 rows in Antarctic polar stereographic projection) were not re-projected or manipulated during this temporal linear interpolation along grid points, which preserved the original spatial resolution.

An additional dataset used in this study was the sea ice motion product of Tschudi *et al.* (2020), which was derived from different passive microwave, visible and infrared satellite observations. These data were not modified and only composites of seasonal (March–October) and long-term (reference period 1981–2010) sea ice drift were aggregated to allow application in this study.

The 30-year annual mean SIC of the SH from 1981 to 2010 was used as a reference period (Figure 2a). The overall pattern is characterized by high annual SIC values in the Weddell Sea, along coastal regions of the Amundsen and Bellingshausen Seas, parts of the Ross Sea, and the Somov Sea. The same pattern was found for the long-term annual mean duration of sea ice cover (Figure 2b). The latter shows the number of consecutive days each pixel is covered by sea ice during the year (SIC > 15%). The Weddell Sea, southern areas of the Amundsen and Bellingshausen Seas, the western Ross and Somov Seas exhibited very long-lasting sea ice cover throughout the year. From this parameter, we defined a domain for the datasets which was subsequently used as input for the cluster classification. The green line in Figure 2b indicates the extent to which the SIC exceeded 15% for at least 30 consecutive days during the reference period 1981–2010. Therefore, the selected input dataset (green dashed box) covers the entire spectrum of sea ice variability, ranging from pixels with no sea ice cover in the most northern areas, to high SIC in the south. With this reduced input dataset the computational effort was reduced because many pixels that were not covered by sea ice were excluded.

2.2 | Cluster classification

The data from the defined classification domain were converted into a matrix containing data for each grid point over 30 years (rows) and 365 days a year (columns).

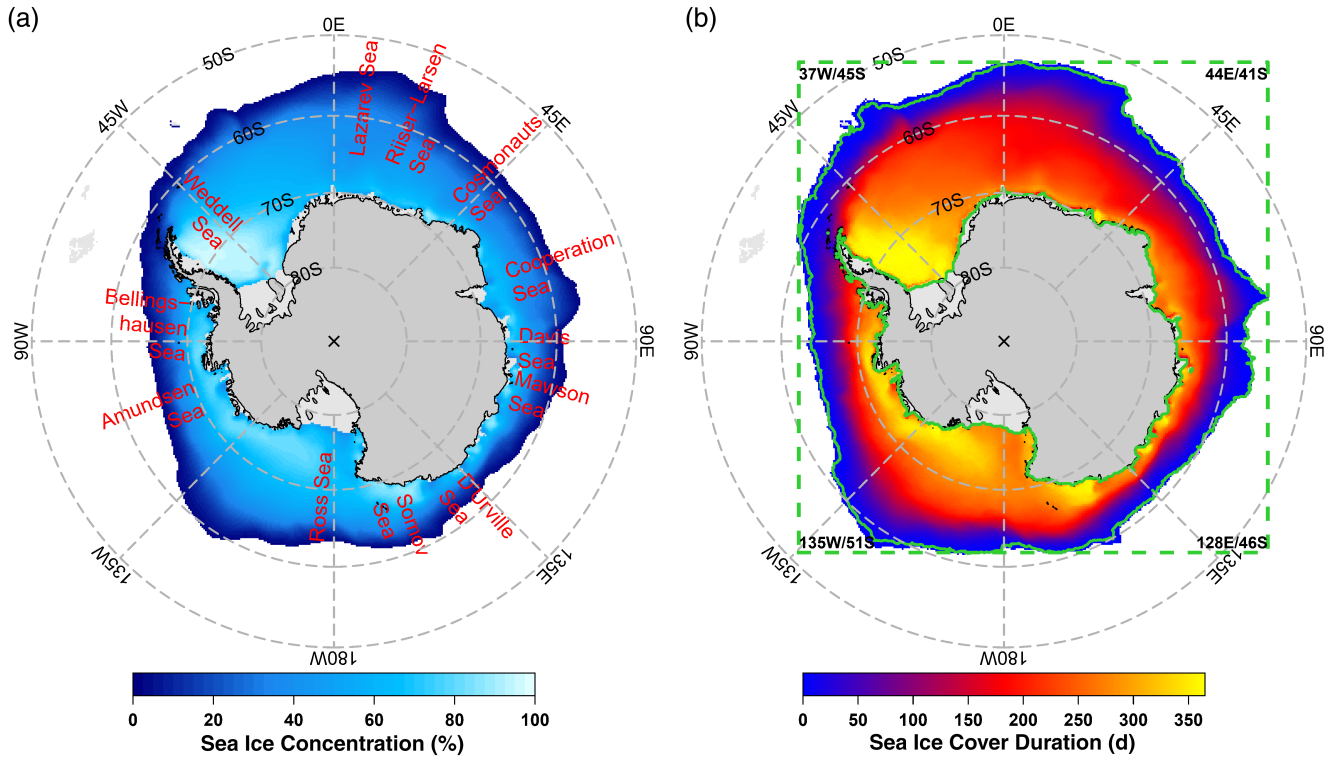

FIGURE 2 (a) Annual averaged SIC of the SH, including the names of relevant Antarctic sea regions; (b) annual averaged continuous sea ice cover duration. The green contour line in (b) indicates the climatological sea ice border (sea ice cover [SIC > 15%] on 30 consecutive days or more)

This data matrix was used as the input for the classification, to derive a climatological reference classification, in which we identified characteristic classes of annual SIC cycles. The classification algorithm applied was the "dkmeans" cluster algorithm, an enhanced version of the k-means clustering method (Hartigan and Wong, 1979), taken from the FORTRAN software package "cost733class" (Philipp *et al*., 2014). Another aspect that needs to be taken into account for this classification is the determination of a certain number of classes. Consequently, classification results with class numbers from 2 to 20 were analysed and interpreted with the aid of the explained variance (EV), and further cluster-quality describing indices. The evaluation of the Faster Silhouette Index (Beck and Philipp, 2010), as well as the Krzanowski-Lai index (Krzanowski and Lai, 1988) and Davies–Bouldin's cluster separation measure (Davies and Bouldin, 1979) from the R software package "clusterSim" (R Core Team, 2017; Walesiak and Dudek, 2017), suggested the use of 10 classes. The EV is a commonly used measure for the quality of the results of classifications or statistical models. For this dataset, EV increased with the number of classes, exceeding 90% at 10 classes, with no further significant increase at higher numbers of classes. The other indices describe the quality of a classification based on measures of the cluster-internal variability and between-cluster separability. The respective index values depend on the number of classes and show minima and maxima, which are used as decision criteria. Through this evaluation, we ensured that a robust setting was defined and that our classification results are representative.

2.3 | Post-classification analysis

The main result of the classification was the identification of 10 significant annual sea ice classes, forming the basis for further investigations. The essential step was the pixel-wise assignment of single annual SIC data to its nearest sea ice class using the least-squares criterion. This individual assignment of annual SIC data allowed an assignment of the same pixel to different classes over the 40-year period according to its inter-annual variability. The nominal class numbers qualitatively represent their mean annual SIC; therefore, the derived classification data set is regarded as an ordinal-scaled data set.

The derived sea ice climatological characterization of the Southern Ocean (Figure 3) describes which class was most frequently identified at a pixel over the 40-year period. A measure of the long-term inter-annual variability was derived by counting the number of different classes at each pixel of the classified data set (Figure 4a). Furthermore, the spatio-temporal variability of sea ice classes allows for an estimation of trends. Since a linear trend calculation on ordinal scaled variables is only a first indicator for trends in the distribution of sea ice classes (Figure 4b), a more advanced trend analysis was applied. The classification results were split into two periods of equal duration: 1979–1998 (Figure 4c) and 1999–2018 (Figure 4d). The compositions of classes of the same regions between the two periods were compared using a Wilcoxon test (significance <0.1). This approach identifies regions of significant shifts towards higher or lower class numbers in the composition of sea ice classes between the two periods.

To analyse inter-annual variability of the sea ice classes, an anomaly dataset of the classification was generated. Using sea ice climatology (Figure 3), the deviations of the classes were determined for each year. Regions with positive (negative) class anomalies indicate classes of higher (lower) orders and thus describe a positive (negative) sea ice anomaly for the corresponding year with a higher (lower) average SIC, respectively. A Climatological Sea Ice Anomaly Index (CSIAI) was developed based on annual class anomalies,*SIa*, to identify years of anomalous cluster deviations. The calculation of the index was mainly based on the areas in which positive (A_{pos}) and negative (A_{neg}) class anomalies were identified. The annual difference between the positive and negative areas was normalized by the total area of the respective region:

$$\mathrm{CSIAI} = \frac{\left(A_{pos} - A_{neg}\right) \cdot \bar{SIa}}{A_{tot}} \tag{1}$$

with

$$\bar{SIa} = \left| \frac{1}{ngp} \sum_{gp=1}^{ngp} SIa(gp) \right| \tag{2}$$

The weighting factor $\bar{SIa}$ over all grid points (*ngp*) strengthens or weakens the area-based term of the CSIAI value according to the sign and intensity of the annual sea ice anomaly. Area-related calculations were performed using the information provided by the National Snow and Ice Data Center (NSIDC) about the exact areas of the pixels.

2.4 | Atmospheric reanalysis data and composites

Composite maps of atmospheric anomalies were derived from ERA-Interim data (Dee *et al*., 2011).

Monthly anomaly fields were calculated as the difference of individual monthly means minus the climatological monthly mean of the reference period 1981–2010. These composites were processed for the months from March to October of each year. These months contain the main annual SIC characteristics, including the advance and the maximum of SIC, and are therefore regarded as the decisive period determining the assignment to a certain sea ice class. Regions of significant anomalous seasonal geopotential height (GPH) and vertical integral of northward total energy flux (VINEF) were identified by applying a Mann–Whitney *U* test with a significance level of 0.1. When comparing seasonal anomalies with long-term conditions, it cannot generally be assumed that the respective samples are normally distributed. Therefore, the nonparametric Mann–Whitney *U* test is preferred, rather than the two-tailed *t* test or Welch test.

3 | RESULTS

3.1 | Sea ice climatology

Figure 3 shows the 10 colour-coded sea ice classes, with the respective annual SIC cycle, for the period 1979–2018, and their geographical distribution around Antarctica. This classification result describes the annual Antarctic sea ice variability over four decades and maps the spatial differentiation of Antarctic sea ice conditions based on the representative seasonal sea ice cycle. The classes were sorted by their mean SIC, with class #1 representing regions of no sea ice coverage and class #10 describing areas with the highest SIC throughout the year (>75% SIC on average). The sea ice classes are arranged zonally around the Antarctic continent, with low SICs in the northern parts of the areas covered by sea ice corresponding to the marginal ice zone, and high SICs further south. While a circumpolar and zonal arrangement of sea ice classes prevails in large parts around Antarctica, a region with classes of higher annual SICs compared to the zonal average was found in the Weddell Sea. In the eastern Weddell Sea and the eastern adjacent sea regions, the mean sea ice motion vectors (arrows in Figure 3) show a considerable zonal component towards the west. This drift direction is interrupted by the Antarctic Peninsula, so that in the western Weddell Sea, sea ice is continuously accumulated and subsequently transported northward along the peninsula. Thus, on the eastern side of the Antarctic Peninsula, sea ice classes with particularly high ice concentrations were found further north than in any other region of the Southern Ocean.

A second interesting and robust result of this classification is the identification of regions of coastal polynyas indicated by black boxes in Figure 3. Here, the general increase in SIC from north to south is not present. These regions, with a predominance of sea ice class #7, are very similar to the circum-Antarctic Polynyas described by Tamura *et al.* (2008). Sea ice class #7 is characterized by a less steep increase and decrease in the SIC during March and October and November. The maximum SIC for class #7 of around 80%, with a variation of ±10%, indicates that even during the Antarctic winter, a significant fraction of open water with SIC around 70% is present, which indicates the presence of coastal polynyas (Tamura *et al.*, 2008; Kern, 2009). Furthermore, the location of class #7 at higher polar latitudes also explains why the SIC does not permanently drop to zero during the summer season. In the southern Ross Sea, the Ross Sea Polynya was identified by this classification approach. Further, smaller polynya regions were found along the east Antarctic coast, the Amundsen and Bellingshausen Seas, the Weddell Sea and Lazarev Sea. These findings can be regarded as a qualitative measure of the sensitivity of the applied classification approach.

3.2 | Spatial Sea ice class variability and trends

Based on the classification results for sea ice classes shown in Figure 3, the long-term variability and trends in the distribution of the sea ice classes were additionally investigated. Inter-annual variability of the sea ice classes is shown in Figure 4a for the period 1979–2018. High values indicate locations where many different classes were identified and where the class variability from year to year was high. Low values represent regions of steady sea ice conditions, with little or no inter-annual variability. These steady regions are the southwestern Weddell Sea and the southern Ross Sea as well as the Riiser-Larsen and Cosmonauts Seas. Regions of high variability are the northern region of the Bellingshausen, Amundsen, Ross, and Somov Seas. Up to eight different classes were identified during the 40 years from 1979 to 2018 in these regions of high variability.

The trend of annual sea ice classes is shown in Figure 4b, based on a linear trend of the class numbers (1–10) over the last 40 years. This analysis does not provide a physically robust description of the quantitative changes in Antarctic sea ice. Nevertheless, it provides a qualitative estimation of regions that have undergone trends, on a climatological time scale, towards higher (lower) class numbers and thus higher (lower) average SIC. These trend patterns are in good accordance with

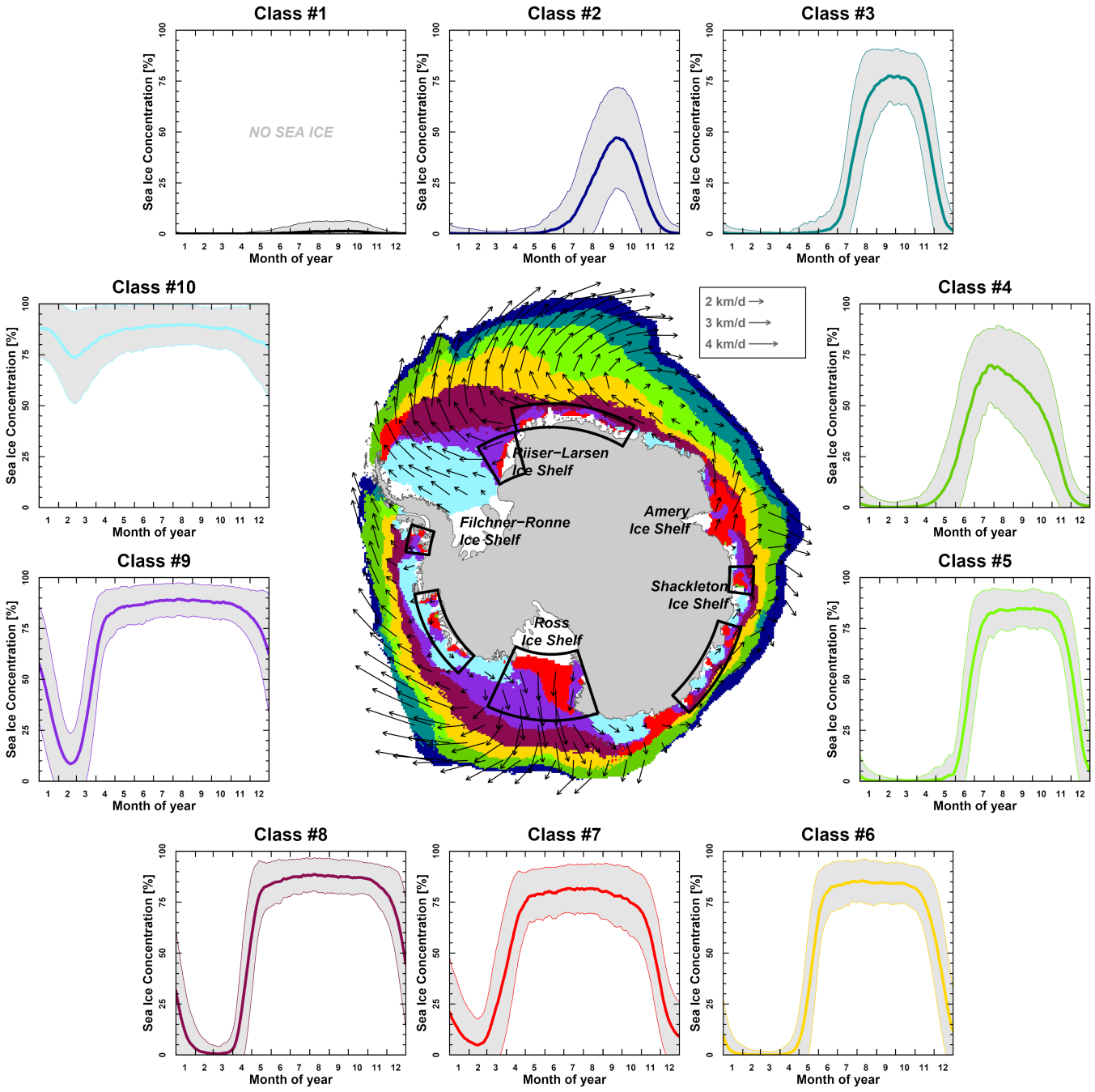

FIGURE 3 Classification results of 40 years (1979–2018) of annual sea ice cycles. The 10 classes are defined by annual SIC patterns. The grey range shows the variability range of the classes (±1 *SD*). The map indicates the regions where the respective classes are located. The Climatological Sea Ice Drift is indicated by black arrows. Black boxes indicate regions overlapping with known polynya regions, which are represented by sea ice class #7. White areas along the Antarctic continent indicate ice shelfs

the documented decrease in SIC in the Bellingshausen and Amundsen Seas (Cavalieri and Parkinson, 2008; Parkinson, 2019).

Figure 4c,d show maps of the most frequently identified classes in the two periods: 1979–1998 and 1999–2018. This classification-based change detection approach shows how annual SIC conditions in different regions of the Southern Ocean have changed during the past four decades. White shaded areas indicate regions with no significant changes in sea ice classes. Significant changes towards classes of higher SICs were found in the Weddell Sea and the adjacent Lazarev and Riiser-Larsen Seas, encircled by bold lines. Sea ice class #10 in the southern central Weddell Sea, with high SICs throughout the year

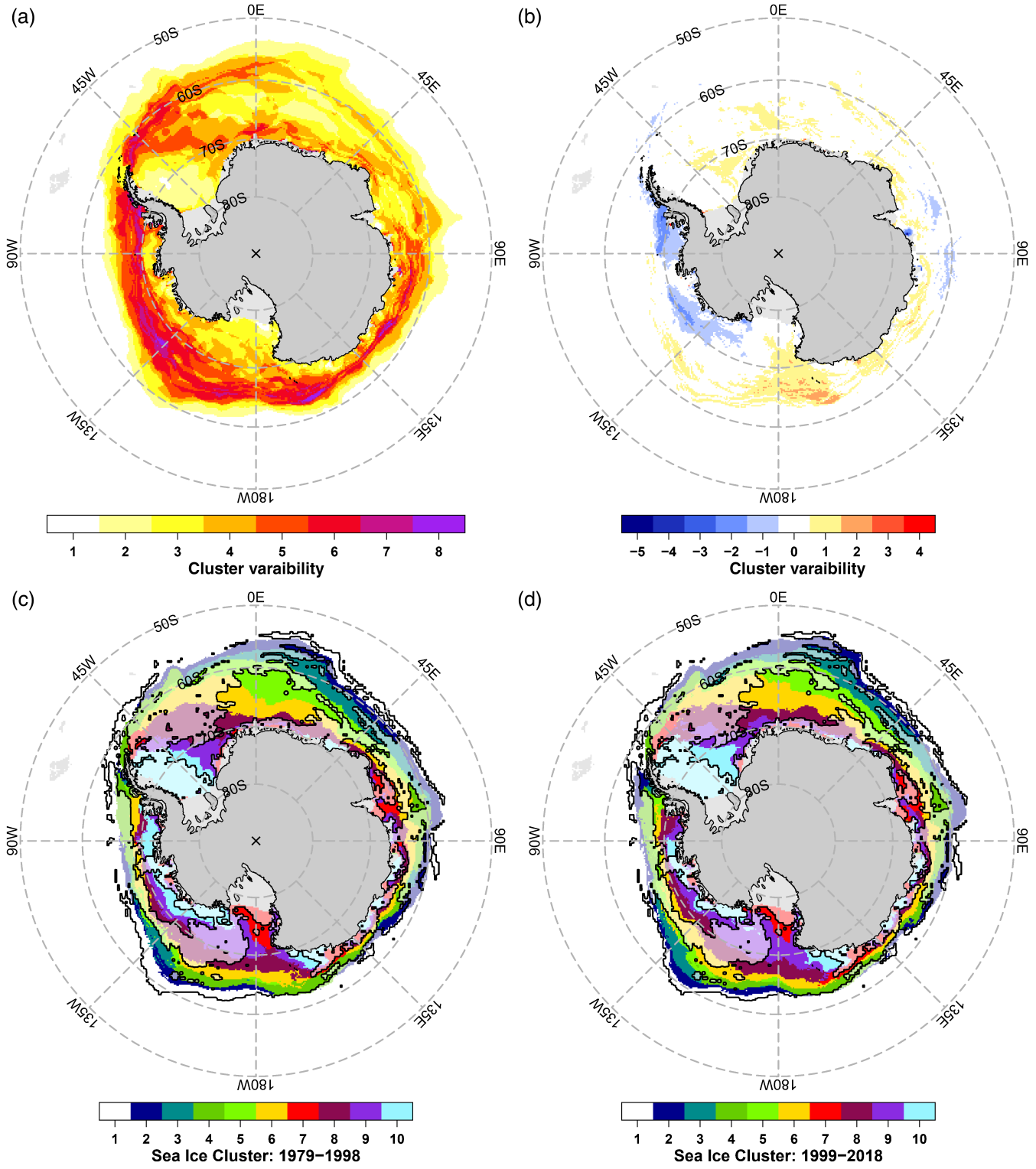

FIGURE 4 (a) Inter-annual variability of the class assignment given in numbers of assigned classes; (b) relative trend of classes towards a higher or lower class number; (c) sea ice classification for the periods 1979–1998 and 1999–2019 in (d). Sea ice classes are colourized as shown in Figure 3. Black contour lines in (c) and (d) indicate regions of significant SIC class changes between the two periods. White shaded regions indicate insignificant differences between the two periods

and only a small summer minimum, expanded eastwards in the central Weddell Sea in regions where sea ice class #9 was predominant in the first period, from 1979 to 1998. The shift towards higher sea ice class numbers is also significant in the eastern Weddell Sea, southern Lazarev, and Riiser-Larsen Seas. Here, we find a

northeastward shift of sea ice classes #9, #8 and #6. This pattern means that the duration of the class-specific summer season with lower SIC was shorter in the second period. Furthermore, the SIC during the summer season did not decline to zero in areas where sea ice class #8 was substituted by class #9, as observed in the southeastern Weddell Sea. The southern Amundsen and Bellingshausen Seas also show significant changes in the dominant classes. Classes #9 and #8, with a longer summer season compared to class #10, were found during the second period in wider areas of the Amundsen and Bellingshausen Seas. The extent of class #10 strongly decreased in the period 1999–2018, and classes #8 and #9 shifted to the southern Amundsen Sea, where class #10 was predominant in the first period. In contrast, the composition of the sea ice classes in the Ross Sea and the Somov Sea developed towards classes of higher numbers, with longer durations of wintertime SIC, and higher SIC during the summer season. Class #9 covered areas, where the Ross Sea Polynya (class #7) was predominant in the first period. Class #8 shifted further north and at the sea ice edge around 150°W class #2 shifted further north, where sea ice was not present during the first period.

3.3 | Inter-Annual Sea ice variability

The CSIAI (see formula (1) in Section 2.3) time series for five different domains across the Southern Ocean is presented in Figure 5. The grey shaded ranges of the CSIAI data indicate the 0.05 and 0.95 percentiles and serve as indicators of years of significant sea ice anomalies. To relate the information given by the CSIAI to the well-known parameter SIE, correlations were calculated for monthly averaged SIE and the respective CSIAI time series for each Antarctic sector. Table 1 indicates that the highest

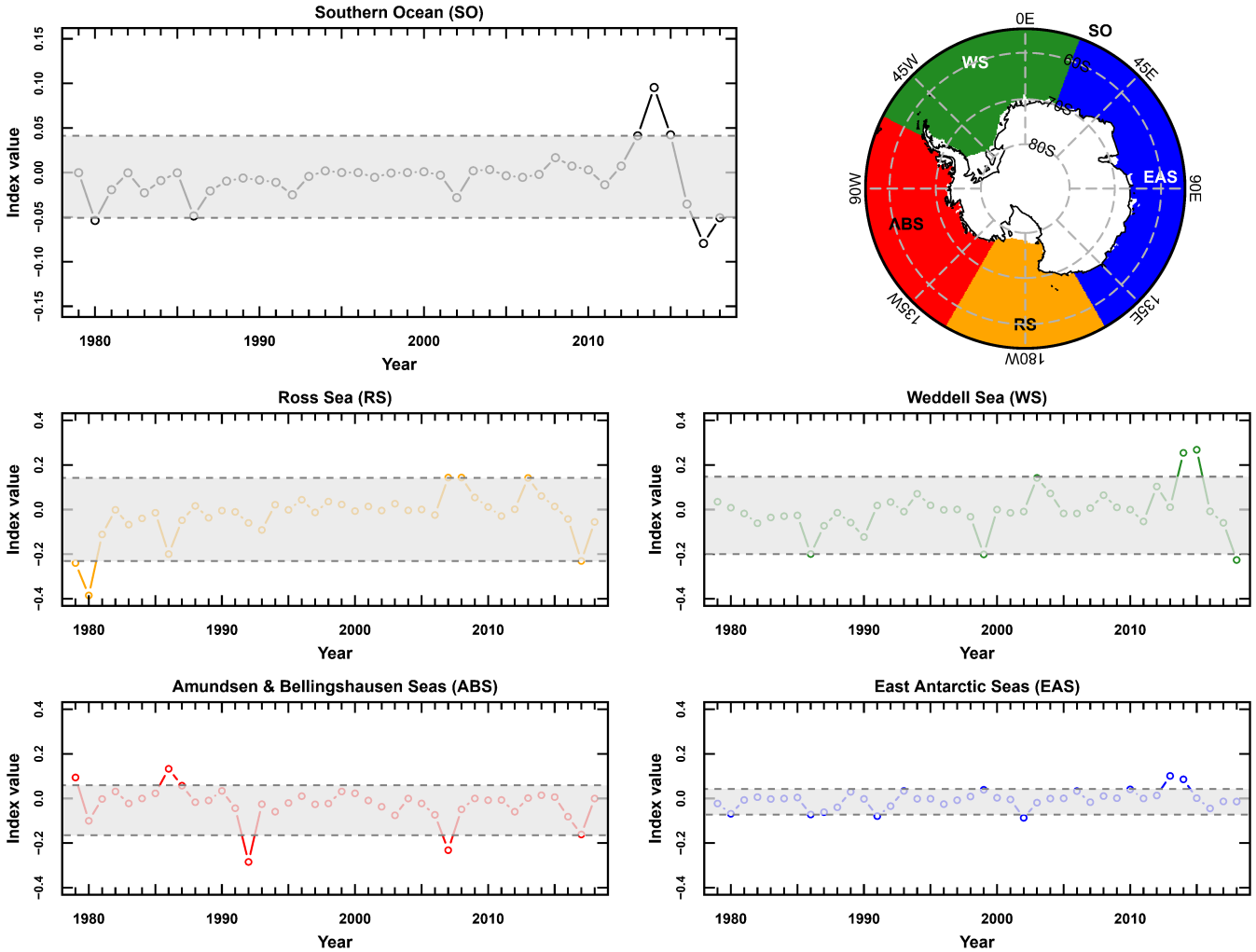

FIGURE 5 Climatological Sea Ice Anomaly Index (CSIAI) time series for five domains: The entire Southern Ocean (south of 55°S) and the four sub-regions Ross Sea (150°E to 150°W), Amundsen and Bellingshausen Seas (150–63°W), Weddell Sea (63°W–20 °E), and the East Antarctic Seas (20–150°E)

TABLE 1 Correlation coefficients between the CSIAI (Figure 5) and the monthly SIE (not shown) for the Southern Ocean and the four Southern Ocean sectors, as indicated in Figure 5

	January	February	March	April	May	June	July	August	September	October	November	December
SO	0.67***	0.66***	0.73***	0.77***	0.83***	0.83***	0.78***	0.68***	0.65***	0.59***	0.59***	0.47**
ABS	0.63***	0.44**	0.46**	0.60***	0.74***	0.73***	0.67***	0.55***	0.45**	0.35*	0.31*	0.35*
WED	0.74***	0.75***	0.73***	0.79***	0.81***	0.72***	0.56***	0.43**	0.37*	0.31*	0.34*	0.40*
EAS	0.47**	0.51***	0.56***	0.63***	0.69***	0.82***	0.81***	0.75***	0.62***	0.63***	0.66***	0.43**
ROS	0.72***	0.64***	0.73***	0.78***	0.80***	0.78***	0.69***	0.41**	0.47**	0.53***	0.55***	0.65***

Note: Asterisks indicate levels of significance derived from a two-sided correlation test after Pearson ($^{*}p < .1$, $^{**}p < .01$, $^{***}p < .001$).

correlations were found during May and June. During these 2 months, classes #4–#6 (Figure 3) are characterized by the advance of sea ice between the summer minimum (no sea ice) and the winter maximum. In the Ross Sea and the Weddell Sea, correlations were higher during the first half of the year. This is because of the presence of sea ice classes (classes #7 and #8 in Figure 3) characterized by an advance of sea ice in the months March and April. For the East Antarctic Seas, high correlations of 0.81 and 0.75 were also found in July and August, reflecting a later sea ice advance of classes #2 and #3, which cover a significant fraction of this sector. The seasonal correlation between CSIAI and SIE shows that the CSIAI is sensitive to the months of sea ice advance and can be interpreted as an indicator of SIE anomalies. Thus, positive (negative) CSIAI values are generally correlated to years with higher (lower) orders of sea ice classes and represent an earlier (later) sea ice advance in the respective regions.

The CSIAI of the entire Southern Ocean exhibited significant negative sea ice anomalies in the years 1980 and 2017 as well as two local minima in 1986 and 2018. Significant positive anomalies were found for the years 2013 until 2015. The extremely positive sea ice anomaly in 2014 was mainly driven by positive anomalies in the Weddell Sea and the East Antarctic Seas. The minima in 2017 and 2018 were induced by sea ice minima in the Ross, Amundsen, Bellingshausen, and Weddell Seas. In 1980, the negative sea ice anomaly in the Ross Sea, as well as below-average conditions in the Amundsen, Bellingshausen, and the East Antarctic Seas, contributed to the significant sea ice minimum in the entire Southern Ocean.

A further interesting pattern of anomalies of Antarctic sea ice variability is the Antarctic dipole (ADP), which was described by Yuan and Martinson (2000). This out-of-phase relationship of sea ice variability between the Pacific and Atlantic basins is part of a pattern of teleconnections connecting tropical and mid-latitude climate variability with variability in Antarctic sea ice (Yuan and Martinson, 2001). In their study, it was shown that remarkable ADP conditions developed in 1980, 1986 and 1992. These anomalies can also be found for these years in Figure 5. Negative anomalies in sea ice were found in the Ross Sea and the Amundsen and Bellingshausen Seas in 1980, while no anomalous sea ice conditions were present in the Weddell Sea. However, in 1986, a strong dipole signal was apparent between the Ross Sea (negative anomaly), the Amundsen and Bellingshausen Seas (positive sea ice anomaly), and the Weddell Sea (negative sea ice anomaly). A pattern of anomalies comparable to that in 1980 was also apparent in 1992. A strong negative sea ice anomaly was apparent in the Amundsen and Bellingshausen Seas, and the

CSIAI indicates below-average sea ice conditions in the Ross Sea. In the Weddell Sea sector, we observed above-average sea ice conditions. According to Yuan (2004), this dipole structure is triggered by warm and cold ENSO events, and it is therefore not a persistent pattern in anomalies of sea ice in the Southern Ocean.

3.4 | Case studies of selected years with patterns of anomalous sea ice

The 2 years 1986 and 2007 (Figures 6 and 7) were investigated in detail, as they represent the sea ice dipole and show relations between anomalous sea ice patterns and the possible influence of atmospheric drivers. Furthermore, the year 2014 (Figure 8) is of special interest since it was the year of most positive CSIAI during the investigation period. These case studies demonstrate the sensitivity of our classification approach and the developed CSIAI to identify atmospheric-induced sea ice anomalies. Figures 6–8 are structured as follows: (a) sea ice class anomaly (relative to the sea ice classification map in Figure 3); (b) seasonal sea ice drift composites (coloured), and the climatological mean sea ice drift of the years 1981 to 2010 as grey vectors; (c) 500 hPa geopotential height (GPH) anomaly composite; and (d) vertical integral of the northward total energy flux anomaly composite (VINEF), as described in Section 2.4. The latter two parameters were included in this study to allow discussion of the influence of seasonal atmospheric drivers on observed sea ice anomalies. The GPH anomalies provide information about anomalies of large-scale atmospheric circulation and the VINEF represents both dynamical and energetic anomalies. The energy fluxes of VINEF are interpreted as a proxy for the meridional transport of air masses. Here, positive northward (negative, southward) directed flux anomalies represent advection of cold polar (warm mid-latitude) air masses. Clearly, however, there are also important oceanic processes that influence the formation of sea ice (e.g., ocean temperatures), as discussed by Meehl *et al.* (2019). In the following, however, the focus is only on large-scale atmospheric conditions.

In 1986, strong negative class anomalies were apparent in the Ross and Somov Sea and in the northern (along 60°S) and eastern (east of 0°E) Weddell Sea sectors (Figure 6a). Particularly in the Ross Sea, a slowed sea ice drift (Figure 6b), and thus a reduced supply of sea ice, caused negative sea ice class anomalies in the northwestern parts of the Ross Sea. Additionally, the atmospheric energy flux, which is directed from mid-latitudes to the south, caused the advection of warm air, which may have enhanced the negative sea ice anomaly due to a reduced production of sea ice. Consequently, lower sea ice classes were found in the Ross Sea. In the Amundsen and Bellingshausen Seas, class numbers above the climatological average were predominant. This opposite effect can also be explained by the meridional energy flux in subpolar latitudes. In the Amundsen and Bellingshausen sectors, this flux was significantly directed from south to north, which supports the formation of sea ice in this region and favours the presence of sea ice at higher latitudes. Large parts of the Weddell Sea exhibited anomalies similar to those of the Ross Sea, which results in less favourable conditions for the formation and persistence of sea ice because of the advection of energy from the Atlantic's mid-latitudes.

The main factor influencing these sea ice and atmospheric energy transport anomalies was a significant positive pressure anomaly over the eastern Ross Sea and the Amundsen Sea (Figure 6c). The quasi-stationary Amundsen-Bellingshausen low, which normally dominates this region, was shifted east, to the northern Antarctic Peninsula, by this significant high-pressure anomaly. On its western side (western Ross Sea and Somov Sea), it allowed the intrusion of warm air masses; on the eastern side, it supported the advection of continental cold air to the north. In the Bellingshausen Sea, this effect was reinforced by a low-pressure anomaly over the northern Antarctic Peninsula. On the eastern side of this low-pressure anomaly (Figure 6c), over the Antarctic Peninsula, more oceanic air reached the central Weddell Sea and led to a negative sea ice anomaly. This advection of warmer mid-latitude air masses was indicated by a negative energy flux anomaly in the Weddell Sea sector (Figure 6d).

The year 2007 (Figure 7) exhibited a nearly opposite pattern in sea ice class anomalies compared to 1986, with higher orders of sea ice classes in the Ross Sea and sea ice classes below the climatological average in the Amundsen and Bellingshausen Seas sector. The main atmospheric driving mechanism was a low-pressure anomaly over the northern Ross Sea sector and an intense high-pressure anomaly over the east Antarctic continent. This pressure anomaly enabled the effective transportation of continental cold air masses over the western Ross and Somov Sea to the north, which is in good agreement with the accelerated northward drift of sea ice in the Ross Sea. Both the advection of cold, continental Antarctic air masses and the accelerated northward sea ice drift probably caused conditions in the western Ross and Somov Seas to favour the production of sea ice. The western Amundsen Sea was affected by the advection of oceanic air masses and less favourable atmospheric conditions for the formation of sea ice. The positive northward energy flux anomaly, apparent in the

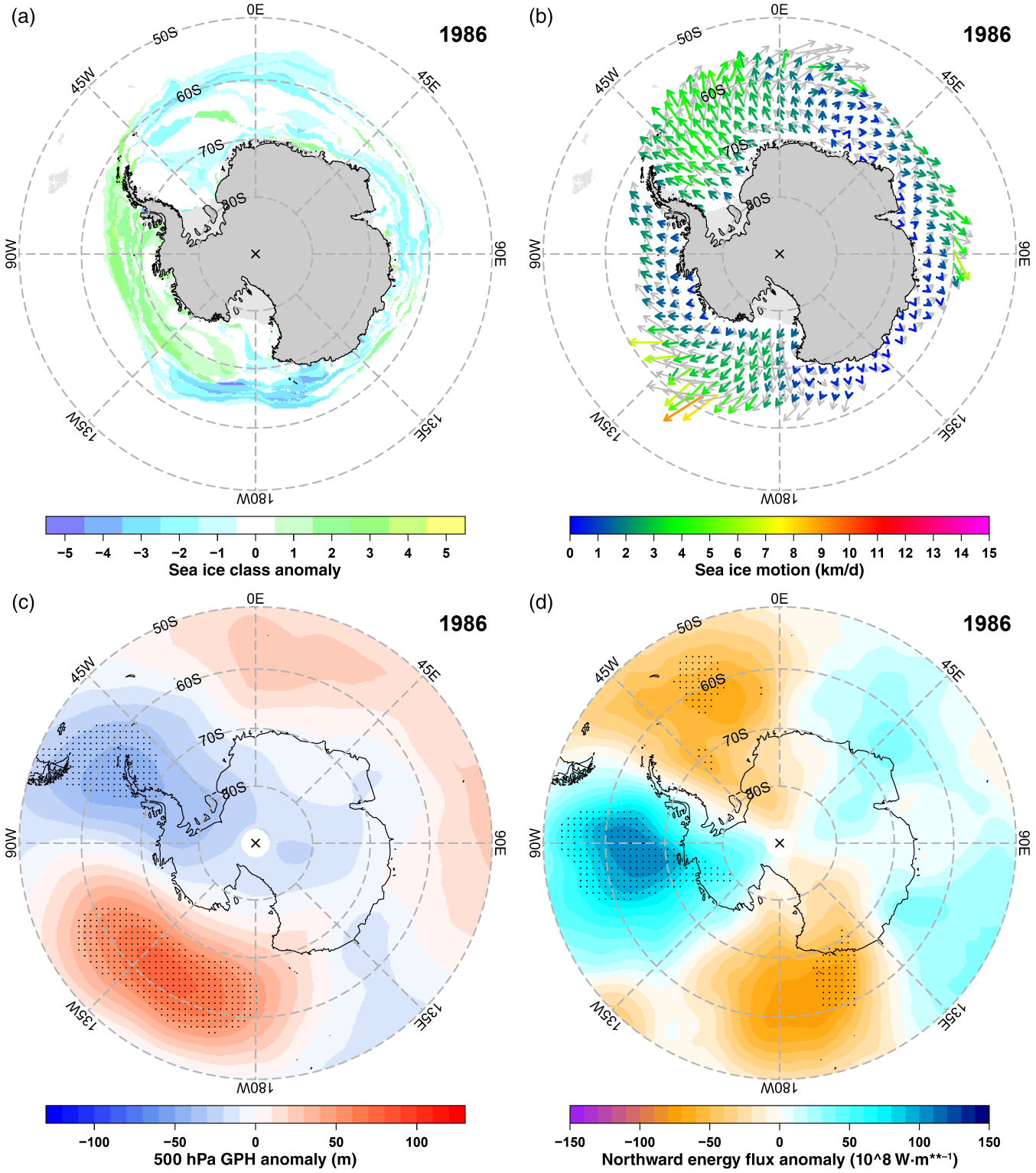

FIGURE 6 Sea ice anomaly and selected atmospheric composites of the year 1986. (a) Sea ice class anomalies; (b) sea ice drift; (c) geopotential height of the 500 hPa level; and (d) vertical integrated northward total energy flux anomaly

eastern Amundsen and Bellingshausen Seas, was not strong enough to produce a positive sea ice anomaly, as was the case in 1986. Therefore, the balance of sea ice was negative in 2007 for the Amundsen and Bellingshausen Seas sector.

During the years 1986 and 2007, significant anomalies in the atmospheric pressure fields were identified, which were associated with meridional energy flux anomalies. These patterns of anomalies, for example, in the southern Pacific, were linked with divergent sea ice anomalies in

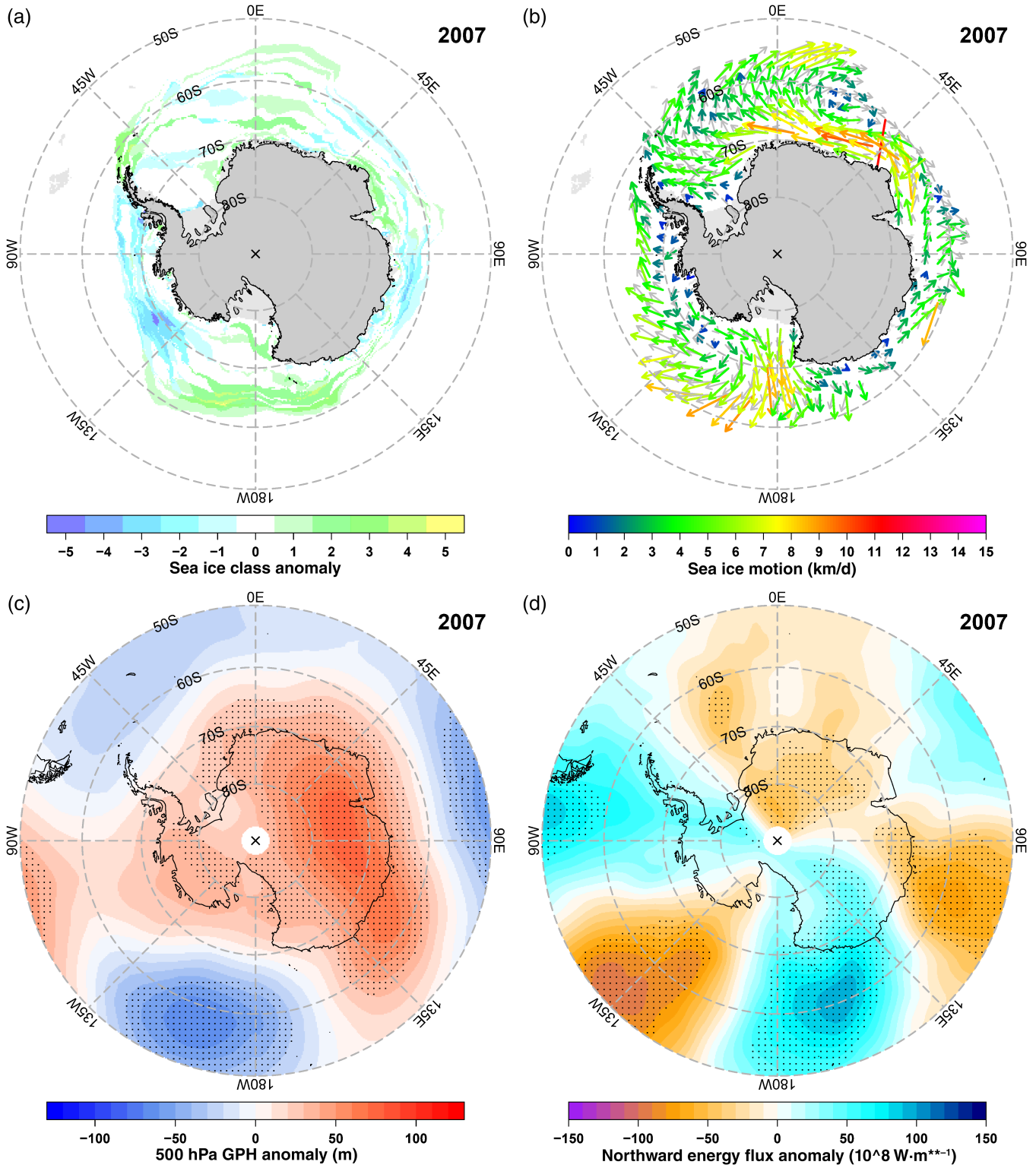

FIGURE 7 Similar analysis as in Figure 6, but for 2007

the Ross, Amundsen, Bellingshausen, and Weddell Sea sectors. In particular, the meridional energy flux showed zonal wavenumber 2 (1986) and zonal wavenumber 3 (2007) structures. In 2014 (Figure 8), no such stationary and inter-seasonally persistent anomaly patterns were identified, which could explain this positive anomaly on a hemispheric scale. Seasonal or sub-seasonal circulation anomalies (Clem *et al.*, 2015) might have played a more important role for the formation of the 2014 sea ice maximum, which cannot be resolved in our atmospheric

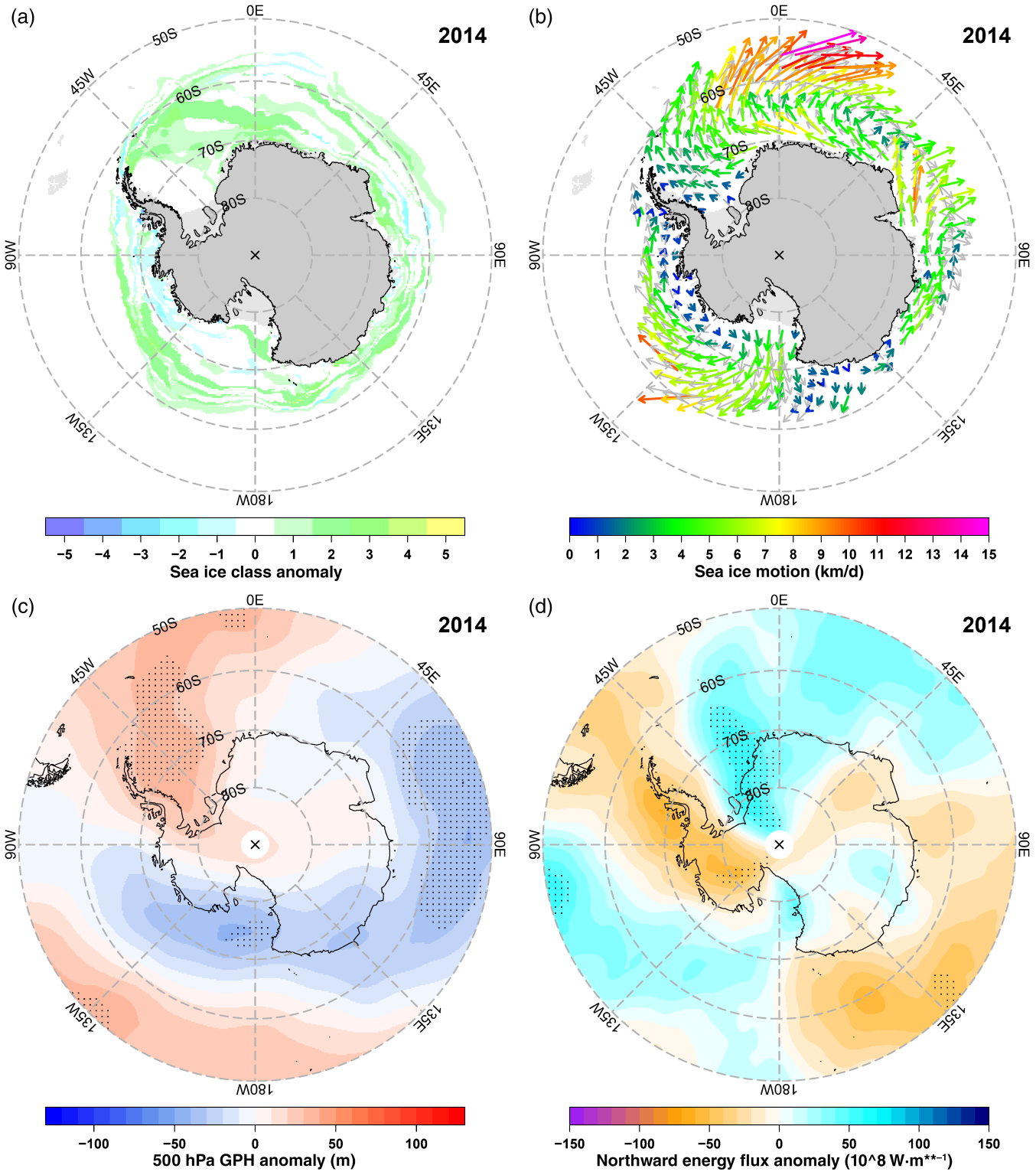

FIGURE 8 Similar analysis as in Figure 6, but for 2014

composites due to the multi-seasonal averaging from March to October. Only the positive GPH anomaly over the western Weddell Sea caused a significant northward energy flux at its eastern side and forced the advection of cold Antarctic air masses towards the central Weddell Sea (Reid *et al.*, 2015a). Another pattern in the GPH anomaly field was a low-pressure anomaly over the central Ross Sea. Because this low-pressure anomaly is located at the same latitudes (between 80 and 70°S) as the Amundsen and Bellingshausen Seas low, one could

speculate whether this anomaly is a westward shifted Amundsen-Bellingshausen low. This low-pressure activity in the central Ross Sea might have driven an intensified northeastern drift of sea ice, which has favoured the formation of sea ice in the Ross Polynya and a dynamically induced positive sea ice anomaly, especially in the northeastern Ross Sea sector. It should also be noted that negative surface temperature anomalies probably have contributed to the positive sea ice anomaly in 2014 (Comiso *et al*., 2017). Another process that favours the formation of sea ice is the freshening of the upper ocean layer as a result of increased precipitation and ocean-induced basal melt of ice shelfs, as it is discussed by Reid *et al*. (2015b) for the above-average sea ice extent in 2013. Such processes might have played also a role for the formation of the sea ice maximum in 2014 and could be subject to further studies on Antarctic sea ice anomalies.

4 | SUMMARY AND OUTLOOK

We presented the method and results of a new cluster classification approach to describe variability in annual sea ice around the Antarctic continent. Our approach consisted of pre-processing the SIC dataset, comprised of both a temporal interpolation (Figure 1) and a first evaluation of long-term sea ice cover (Figure 2). Based on these results, a representative domain was selected, serving as the basis for further classification. For this purpose, a sensitivity study was conducted to define a suitable number of classes for the selected "dkmeans" classification method. The 10 identified annual sea ice classes, in combination with the spatial assignment to individual pixels and years of the original dataset, enabled the classification of an Antarctic sea ice climatology based on 40 years of passive microwave remote sensing data (Figure 3). This method included an annual classification of the spatial distribution of our annual sea ice classes, which also allowed for the identification of trend patterns of sea ice classes over the last four decades (Figure 4). Furthermore, our newly developed Climatological Sea Ice Anomaly Index (CSIAI) highlighted the particular years of anomalous Antarctic sea ice variability (Figure 5). Both the phenomenon of the ADP and years of extreme sea ice extent (max. SIE in 2014, min. SIE in 2017) were reliably identified by the CSIAI. Additionally, years of remarkable annual sea ice class anomalies were linked to significant circulation anomalies in the troposphere (Figures 6–8).

As is the case for any data classification method, this classification also led to a generalization and condensation of information, namely into 10 annual sea ice classes and their annual or long-term patterns of spatial distribution. The annual sea ice classes include characteristic properties of intra-annual SIC variability, including the minimum and maximum sea ice concentrations and the duration of the summer and winter sea ice season, respectively. The identification of a specific class, which was mainly overlapped with known polynya regions, demonstrated the good performance of our classification method in comprehensively capturing variability in intra-annual sea ice over the entire Southern Ocean. From the results presented above, we conclude that our method provides a suitable tool for reviewing spatial Antarctic sea ice variability on annual to multi-decadal time-scales. Therefore, the methodology could also be applied to the results of sea ice models in future studies. Due to the high climatological representativeness of the derived annual sea ice classes, they could also serve as a reference for the evaluation of models. Furthermore, it could be examined whether this classification method, when applied analogously to model results, delivers similar annual sea ice classes. Finally, the sea ice classes generated in this study could be directly assigned to model data to investigate whether these models are capable of reproducing the observed patterns in the spatial distribution and temporal shifts of SIC classes and additional patterns, including the ADP.

ACKNOWLEDGEMENTS

The authors would like to gratefully acknowledge the financial support and endorsement from the DLR Management Board Young Investigator Group Leader Program and the Executive Board Member for Space Research and Technology. F.R. is funded by the Deutsche Forschungsgemeinschaft (DFG) in the framework of the priority program "Antarctic Research with comparative investigations in Arctic ice areas" under Grants HE 2740/22 and WI 3314/3.

We acknowledge the European Centre for Medium-Range Weather Forecasts for providing the ERA-Interim data. The National Snow and Ice Data Center is acknowledged for the provision of sea ice concentration data and sea ice motion data.

We greatly appreciate the valuable feedback from three anonymous reviewers. Open access funding enabled and organized by Projekt DEAL.

ORCID

Paul Wachter https://orcid.org/0000-0002-8303-1675
Fabian Reiser https://orcid.org/0000-0003-1128-8452

REFERENCES

Beck, C. and Philipp, A. (2010) Evaluation and comparison of circulation type classifications for the European domain. *Physics and Chemistry of the Earth*, 35, 374–387.

Cavalieri, D.J. and Parkinson, C.L. (2008) Antarctic Sea ice variability and trends, 1979–2006. *Journal of Geophysical Research*, 113, C07004.

Cavalieri, D.J., Parkinson, C.L., Gloersen, P. and Zwally, H.J. (1996) *Sea ice concentrations from Nimbus-7 SMMR and DMSP SSM/I-SSMIS passive microwave data. Version 1.1, updated yearly*. Boulder, Colorado USA: NASA National Snow and Ice Data Center Distributed Active Archive Center https://doi.org/10.5067/8GQ8LZQVL0VL [Accessed 21st March 2019].

Clem, K.R., Barreira, S. and Fogt, R.L. (2015) Atmospheric circulation [in "state of the climate in 2014"]. *Bulletin of the American Meteorological Society*, 96(7), 149–151.

Comiso, J.C., Gersten, R.A., Stock, L.V., Turner, J., Perez, G.J. and Cho, K. (2017) Positive trend in the Antarctic Sea ice cover and associated changes in surface temperature. *Journal of Climate*, 30, 2251–2267.

Davies, D.L. and Bouldin, D.W. (1979) A cluster separation measure. *IEEE Transactions on Pattern Analysis and Machine Intelligence.*, 1(2), 224–227.

Dee, D.P., Uppala, S.M., Simmons, A.J., Berrisford, P., Poli, P., Kobayashi, S., Andrae, U., Balmaseda, M.A., Balsamo, G., Bauer, P., Bechtold, P., Beljaars, A.C.M., van de Berg, L., Bidlot, J., Bormann, N., Delsol, C., Dragani, N.R., Fuentes, M., Geer, A.J., Haimberger, L., Healy, S.B., Hersbach, H., Holm, E.V., Isaksen, L., Kallberg, P., Kohler, M., Matricardi, M., McNally, A.P., Monge-Sanz, B.M., Morcrette, J.J., Park, B.K., Peubey, C., de Rosnay, P., Tavolato, C., Thepaut, J.N. and Vitart, F. (2011) The ERA-interim reanalysis: configuration and performance of the data assimilation system. *Quarterly Journal of the Royal Meteorological Society*, 137, 553–597.

Eicken, H. (1992) The role of sea ice in structuring Antarctic ecosystems. In: Hempel, G. (Ed.) *Weddell Sea Ecology*. Berlin, Heidelberg: Springer.

Gordon, A.L., Visbeck, M. and Comiso, J.C. (2007) A possible link between the Weddell Polynya and the southern annular mode. *Journal of Climate*, 20, 2558–2571.

Hartigan, J.A. and Wong, M.A. (1979) Algorithm AS 136: a k-means clustering algorithm. *Journal of the Royal Statistical Society: Series C (Applied Statistics)*, 28, 100–108.

Hobbs, W.R., Massom, R., Stammerjohn, S., Reid, P., Williams, G. and Meier, W. (2016) A review of recent changes in Southern Ocean sea ice, their drivers and forcings. *Global and Planetary Change*, 143, 228–250.

Holland, P.R. and Kwok, R. (2012) Wind-driven trends in Antarctic Sea-ice drift. *Nature Geoscience*, 5, 872–875.

Kern, S. (2009) Wintertime Antarctic coastal polynya area: 1992–2008. *Geophysical Research Letters*, 36, 14501.

King, J.C. and Turner, J. (1997) *Antarctic Meteorology and Climatology*. Cambridge: Cambridge University Press.

Krzanowski, W.J. and Lai, Y.T. (1988) A criterion for determining the number of groups in a data set using sum of squares clustering. *Biometrics*, 44, 23–34.

Maykut, G.A. (1982) Large-scale heat exchange and ice production in the Central Arctic. *Journal of Geophysical Research*, 87, 7971–7984.

Meehl, G.A., Arblaster, J.M., Chung, C.T.Y., Holland, M.M., DuVivier, A., Thompson, L., Yang, D. and Bitz, C.M. (2019) Sustained Ocean changes contributed to sudden Antarctic Sea ice retreat in late 2016. *Nature Communications*, 10, 14.

Parkinson, C.L. (2019) A 40-y record reveals gradual Antarctic Sea ice increases followed by decreases at rates far exceeding the rates seen in the Arctic. *PNAS*, 116, 14414–14423.

Philipp, A., Beck, C., Huth, R. and Jacobeit, J. (2014) Development and comparison of circulation type classifications using the COST 733 dataset and software. *International Journal of Climatology*, 36, 2673–2691.

R Core Team. (2017) *R: A Language and Environment for Statistical Computing*. Vienna, Austria: R Foundation for Statistical Computing https://www.R-project.org/.

Reid, P., Massom, R.A., Stammerjohn, S., Barreira, S., Scambos, T. and Lieser, J.L. (2015a) Sea ice extent, concentration, and duration [in "state of the climate in 2014"]. *Bulletin of the American Meteorological Society*, 96(7), 160–165.

Reid, P., Stammerjohn, S., Massom, R., Scambos, T. and Lieser, J. (2015b) The record 2013 Southern Hemisphere Sea-ice extent maximum. *Annals of Glaciology*, 56(69), 99–106.

Schlosser, E., Haumann, F.A. and Raphael, M.N. (2018) Atmospheric influences on the anomalous 2016 Antarctic Sea ice decay. *The Cryosphere*, 12, 1103–1119.

Sigmond, M. and Fyfe, J.C. (2014) The Antarctic Sea ice response to the ozone hole in climate models. *Journal of Climate*, 27, 1336–1342.

Simmonds, I. and Jacka, T.H. (1995) Relationships between the interannual variability of Antarctic Sea ice and the southern oscillation. *Journal of Climate*, 8, 637–647.

Simpkins, G.R., Ciasto, L.M. and England, M.H. (2013) Observed variations in multidecadal Antarctic Sea ice trends during 1979-2012. *Geophysical Research Letters*, 40, 3643–3648.

Smith, S.D., Muench, R.D. and Pease, C.H. (1990) Polynyas and leads: an overview of physical processes and environment. *Journal of Geophysical Research*, 95, 9461–9479.

Stammerjohn, S.E., Martinson, D.G., Smith, R.C., Yuan, X. and Rind, D. (2008) Trends in Antarctic annual sea ice retreat and advance and their relation to El Niño–southern oscillation and southern annular mode variability. *Journal of Geophysical Research*, 113, C03S90.

Stuecker, M.F., Bitz, C.M. and Armour, K.C. (2017) Conditions leading to the unprecedented low Antarctic Sea ice extent during the 2016 austral spring season. *Geophysical Research Letters*, 44, 9008–9019.

Tamura, T., Ohshima, K.I. and Nihashi, S. (2008) Mapping of sea ice production for Antarctic coastal polynyas. *Geophysical Research Letters*, 35, L07606.

Tschudi, M.A., Meier, W.N. and Stewart, J.S. (2020) An enhancement to sea ice motion and age products at the National Snow and ice data center (NSIDC). *Cryosphere*, 14, 1519–1536 [access 18th June 2019].

Turner, J., Comiso, J.C., Marshall, G.J., Lachlan-Cope, T.A., Bracegirdle, T., Maksym, T., Meredith, M.P., Wang, Z. and Orr, A. (2009) Non-annular atmospheric circulation change induced by stratospheric ozone depletion and its role in the recent increase of Antarctic Sea ice extent. *Geophysical Research Letters*, 36, L08502.

Turner, J., Guarino, M.V., Arnatt, J., Jena, B., Marshall, G.J., Phillips, T., Bajish, C.C., Clem, K., Wang, Z., Andersson, T., Murphy, E.J. and Cavanagh, R. (2020) Recent decrease of summer sea ice in the Weddell Sea, Antarctica. *Geophysical Research Letters*, 47, L087127.

Turner, J., Hosking, J.S., BracegirdleTJ, M.G.J. and Phillips, T. (2015) Recent changes in Antarctic Sea ice. *Philosophical Transactions of the Royal Society A*, 373, 20140163. https://doi.org/10.1098/rsta.2014.0163.

Turner, J., Phillips, T., Marshall, G.J., Hosking, J.S., Pope, J.O., Bracegirdle, T.J. and Deb, P. (2017) Unprecedented springtime retreat of Antarctic Sea ice in 2016. *Geophysical Research Letters*, 44, 6868–6875.

Van den Broeke, M. (2000) The semi-Aannual oscillation and Antarctic climate. Part 4: a note on sea ice cover in the Amundsen and Bellingshausen seas. *International Journal of Climatology*, 20, 455–462.

Walesiak, M., Dudek A. (2017). clusterSim: Searching for Optimal Clustering Procedure for a Data Set. R package version 0.47–1. https://CRAN.R-project.org/package=clusterSim.

Yuan, X. (2004) ENSO-related impacts on Antarctic Sea ice: a synthesis of phenomenon and mechanisms. *Antarctic Science*, 16, 415–425.

Yuan, X. and Martinson, D.G. (2000) Antarctic Sea ice extent variability and its global connectivity. *Journal of Climate*, 13, 1697–1717.

Yuan, X. and Martinson, D.G. (2001) The Antarctic dipole and its predictability. *Geophysical Research Letters*, 28, 3609–3612.

Zwally, H.J., Comiso, J.C., Parkinson, C.L., Cavalieri, D.J. & Gloersen, P. (2002) Variability of Antarctic Sea ice 1979–1998. *Journal of Geophysical Research*, 107(C5), 9-1–9-19.

How to cite this article: Wachter P, Reiser F, Friedl P, Jacobeit JA new approach to classification of 40 years of Antarctic sea ice concentration data. *Int J Climatol*. 2021;41 (Suppl. 1):E2683–E2699. https://doi.org/10.1002/joc.6874